Assembly of π-Conjugated Helical Peptides into a Porous and Evolvable Protein-like Lattice

Sherrie L. Heinz-Kunert,[a,‡] Ashma Pandya,[a,‡] Viet Thuc Dang,[a] Phuong Nguyen Tran,[a] Sabari Ghosh,[a] Dan McElheny,[a] Bernard D. Santarsiero,[b] Zhong Ren,[a] Andy I. Nguyen[a,*]

[a] Department of Chemistry, University of Illinois at Chicago, Chicago, Illinois 60607, United States

[b] Department of Pharmaceutical Sciences, University of Illinois at Chicago, Chicago, Illinois 60607, United States.

ABSTRACT: The evolution of proteins from simpler, self-assembled peptides provides a powerful blueprint for the design of complex synthetic materials. Previously, peptide–metal frameworks using short sequences (≤ 3 residues) have shown great promise as proteomimetic materials that exhibit sophisticated capabilities. However, their evolution has been hindered due to few mutable residues and restricted choice of side-chains that are compatible with metal ions. Herein, we developed a non-covalent strategy using π-stacking to assemble much longer peptides into crystalline frameworks that tolerate even previously incompatible acidic and basic functionalities, and allow an unprecedented level of pore mutations. Single-crystal X-ray structures are provided for all mutants to guide and validate rational design. These materials exhibit hallmark protein behaviors such as guest-selective induced-fit and assembly of multi-metallic units. Significantly, we demonstrate facile evolution of the framework to substantially increase affinity towards a complex organic molecule.

Tailored microenvironments allow efficient execution of important functions such as catalysis or selective binding. Though they are usually challenging to make in synthetic molecules, evolution has produced an enormous diversity of proteins bearing channels and cavities that can engage substrates with dynamic motions and precise ensembles of functional groups.[1] Despite the sophistication of modern-day proteins, strong evidence suggest that they evolved from self-assembled aggregates of shorter, simpler peptides(<50 amino acids[2]).[3–7] This evolutionary hypothesis is an attractive synthetic blueprint for designing complex and dynamic materials for catalysis, separations, and drug delivery, and could fill a key gap between small molecule and protein assemblies.[8–12] Moreover, peptides and peptidomimetics are especially modular and efficient to synthesize by the technique of solid-phase peptide synthesis (SPPS), which makes them powerful building blocks.[13–15]

Towards this end, peptide-metal frameworks made from short peptides (with 3 or fewer amino acids) have made remarkable advances, achieving complex pores that can discriminate between chiral substrates, exhibit dynamic behavior, and perform catalysis.[16–29] Moving forward, longer peptides could allow greater variability and functionality, but control of secondary structure becomes a critical barrier. As a result the longest peptide known to support a porous coordination framework is based on Pro_6, which leverages the unique rigidity of proline.[16] More importantly, evolution of the pores, which requires having mutable sites, remains underdeveloped likely due to the limitations associated with both short peptides and metal-coordination bonds. The few amino acid positions not involved in connecting the metal nodes (usually only one, thus far) poorly tolerate functionally-important polar side-chains (e.g. those bearing a carboxylic acid, N-donors, or S-donors) that potentially interfere with metal binding, while mutations to non-polar residues tend to drastically re-structure the topology of the framework since they are involved in key packing interactions.[23,25,30–34]

The use of longer peptides would greatly enhance evolvability of peptide-frameworks, but it involves both the endeavor of de novo peptide design and engineering of weaker interactions. Non-covalent porous peptide lattices are rare, and their design rules and supramolecular reactivity are less established.[35–39] Thus, there is a need for the rational design of non-covalent peptide frameworks, from which sequence variations can lead to the rapid evolution of sophisticated porous materials.

Herein, we show that non-covalent, metal-free assembly of π-conjugated peptides (peptides hybridized with extended aromatic moieties) can reliably form frameworks with highly variable, nanometer-sized pores lined with functionality from six different residues. These materials are stable in water and several organic solvents and allow rational pore mutagenesis at three different sites, tolerating even acidic and basic functional groups. The frameworks are multifunctional, capable of hosting organic and inorganic molecules. Crucially, we demonstrate that evolution is easily accomplished, as illustrated by discovery of variant with high affinity for a complex organic guest.

RESULTS AND DISCUSSION

In order to construct functionally rich, porous peptide frameworks that persist in a variety of environments, we incorporated several design elements (Figure 1a): a stable secondary and tertiary structure building block, hydrophobic π-stacking residues to generate a lattice,[40] and a number of mutable positions that point into the pore space. We targeted an α-helical secondary structure as it provides many unique positions for tuning enabled by the regular

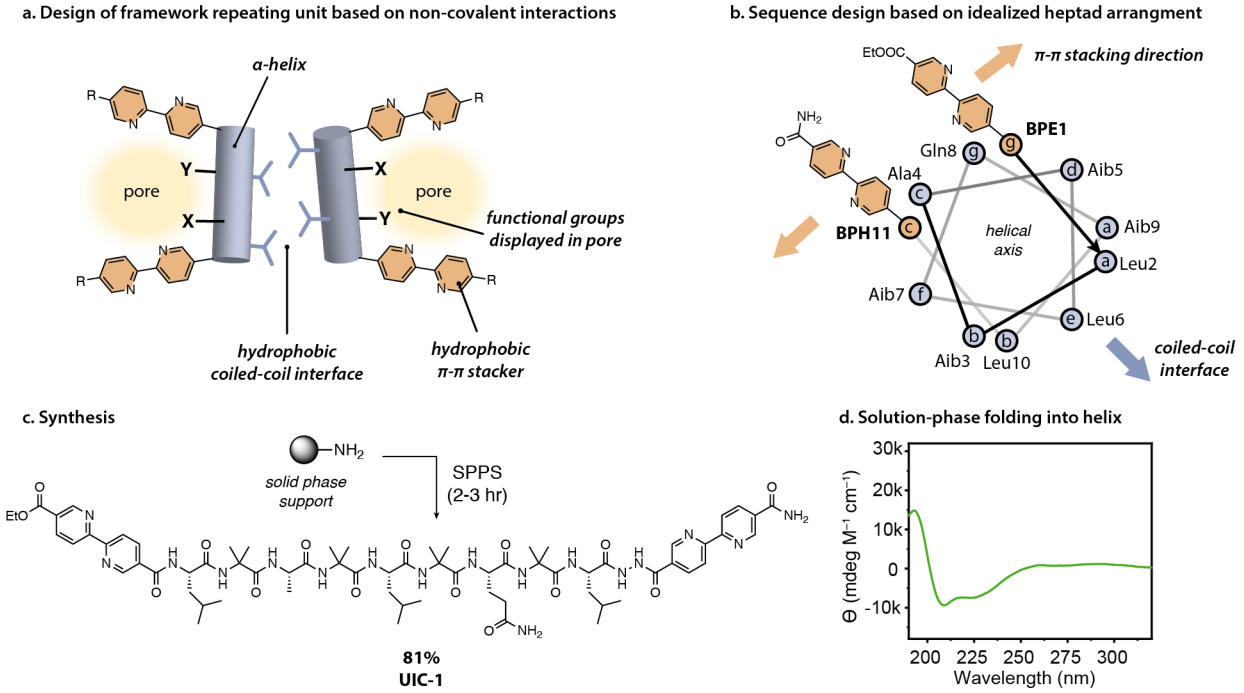

Figure 1. (a) Conceptual design of a network-generating building block. (b) Using an ideal α-helix geometry, residues were placed to enforce desired intermolecular interactions. (c) Synthesis of **UIC-1** by solid-phase peptide synthesis (SPPS). (d) CD spectrum of **UIC-1** in 1:9 H_2O:MeCN showing α-helical structure.

heptad arrangement of side chains (Figure 1b).[41,42] To reliably enforce helicity, we leveraged the conformational rigidity of the non-canonical amino acid, 2-aminoisobutyric acid (Aib or B), which is known to strongly induce folding into a 3_{10} or α-helix, with the latter being favored in longer peptides.[43,44] Considering the arrangement of side-chains in an idealized α-helix (Figure 1b), positions *a* and *d* were chosen to display hydrophobic side chains derived from Leu or Aib to favor coiled-coil formation.[45] To further promote lateral growth of the coiled-coils, positions *b, e,* and *g* were chosen to feature residues that have strong intermolecular interactions. In position *b* and *e*, Leu and Aib were selected to promote hydrophobic packing, while adding Gln in position *g* could introduce interchain H-bonding. This leaves positions *c* and *f* theoretically pointing into the pores and are possible sites for pore engineering.

Rigid, planar bipyridyl residues, BPE and BPH, cap the helix in positions *c* and *g*, respectively (Figure 1b, 1c), and are intended to be roughly perpendicular to the helical axis to provide sites for π-stacking, and the pores are to be generated upon association with other π-stacked units. A coiled-coil interaction would produce two opposed pairs of bipyridyl moieties that can grow the lattice by π-π-stacking. Peptides conjugated with large aromatic moieties have been shown to reliably engage in π-π stacking to form 1-D and 2-D extended assemblies, but a 3-D assembly has not yet been demonstrated.[46–49] Our design principles are culminated in the peptide sequence, **UIC-1** (Figure 1c). **UIC-1** was synthesized by SPPS (SI), which provided pure compound in ~1 day with 81% yield. As intended, **UIC-1** strongly folds into a helical structure in a 1:9 H_2O: MeCN solution as confirmed by circular dichroism (Figure 1d) and 2D NMR spectroscopy (Supporting Information).[43]

UIC-1 is poorly soluble in pure water or MeCN but shows slightly improved solubility in 1:9 H_2O: MeCN with a large temperature dependence. Crystalline blocks of **UIC-1** were obtained from slow cooling of a refluxing saturated solution in 1:9 H_2O: MeCN (SI for details). Single crystal X-ray diffraction (SC-XRD) of **UIC-1** reveals a lattice of large, rectangular, infinite channels (widths of 1.5 x 1.1 nm) running along the *b* direction ($P2_1$ space group, a=13.797 Å, b=13.456 Å, c=27.690 Å, α=90.00° β=99.58° γ=90.00°). In line with our design goals, π-π interactions, mediated by BPE and BPH, are a prominent feature of the framework, along with antiparallel coiled-coil interactions.

There are several key characteristics of this framework. Firstly, the structure of the peptide monomer exhibits a mixture of helical folds: α-helix between residues 2–7 and a more tightly twisted 3_{10}-helix between residues 7–9, with a slight bend at the junction of the two domains (Fig. 2b) that is stabilized by an unforeseen intramolecular H-bond between the side-chain of Gln8 and the carbonyl oxygen of Aib5. This serendipitous helical distortion allows BPH and BPE to adopt nearly parallel orientations that maximize π-π contacts. Secondly, running down the *b* axis are rows of alternating, interdigitated BPH and BPE residues. The two rings within the bipyridyl unit are essentially coplanar, and the average interplanar distance between stacked BPH and BPE is 3.4 Å, typical of parallel π-π stacking (Figure 2d).[50] The π-stacked rows are spaced along the *a* axis with the closest ring–ring distance of 1.36 nm, and are a significant structural element as it connects chains along the three crystallographic axes. The connection of the peptide chains via the π stacks form a shelf-like substructure of the framework. These shelf-like units are arranged along the *c* direction via antiparallel coiled-coil packing of Leu and Aib residues to generate the full framework. Interestingly, the designed lateral coiled-coil interactions (helical positions *b* and *e*) did not manifest, leading to large cavities between adjacent helices (Figure 2c) that are occupied by MeCN molecules. These cavities branch from the main channel of the framework further augmenting

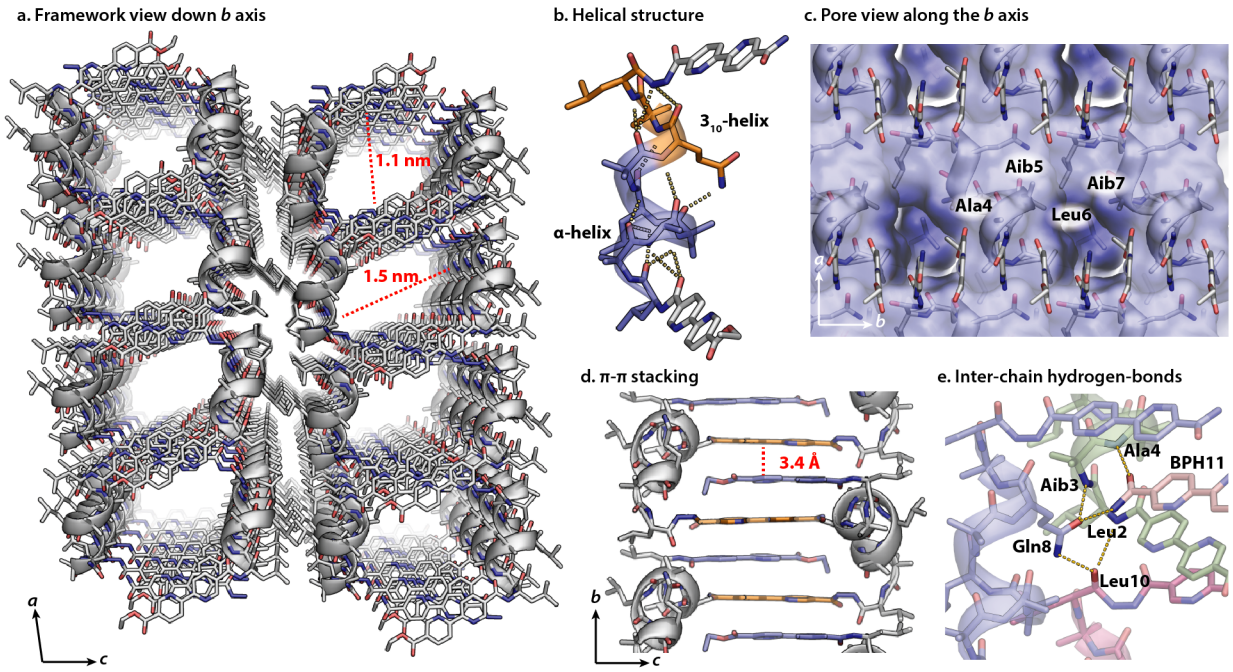

Figure 2. X-ray crystal structure of **UIC-1**. Solvent molecules (water and MeCN), and hydrogen atoms have been omitted for clarity. (a) Overview of framework demonstrating the infinite channels. Pore widths are measured from (BPE C18 to BPE C18, and B5 HB11 to B5 HB12) indicated in red dashed lines. α-helical regions are depicted using ribbons while gray, red, and blue rods designate carbon, oxygen, and nitrogen atoms respectively. (b) View of the peptide helical building block. Blue region denotes the α-helix domain, and the orange region denotes the 3_{10}-helix domain. Yellow dashed lines indicate H-bonds within the chain. (c) View of the channel along the *b*-axis to show the minor pores (shaded in darker blue). Amino acid residues defining the pore are labeled in white. (d) A section of the π-π stacking column; BPH (blue) and BPE (orange). (e) Residues involved in hydrogen-bonds between separate chains.

the complexity of the porous structure. Lastly, networks of inter-chain H-bonding contribute to the stability of the framework and occurs in three instances (Figure 2e): (1) between neighboring chains (side-chain of Gln8 and the backbone of Leu10), (2) across the pore (carboxamide of BPH with both side-chain of Gln8 and Ala4), and (3) between the helical termini (side-chain of Gln8 and backbone of Aib3, and backbones of Leu10 and Leu2). Thus, the sidechain of Gln8 plays a critical role, engaging in three different interchain and one intrachain (*vide supra*) H-bonding interactions.

The composition of the pore is remarkable in that it is defined by six unique residues – BPE1, A4, B5, L6, B7, and BPH11 – which allows potential for the pore to be unprecedently modular. Previous examples of peptide–metal frameworks could, at most, allow isoreticular mutations in one position, but most examples of mutations result in totally different framework topologies.[17,18,21,24,31,51,52] We predicted that **UIC-1** may be more rationally mutated to introduce new functional groups while preserving the general framework architecture since it is based on a longer peptide (9 amino acids) and its sidechains at positions at 4, 5, and 7 point unobstructed into the pore (Figure 3a). Those positions were mutated to a variety of amino acids that represent the breadth of functional group sterics and electronics: thioether (Met), hydroxyl (Ser), aromatic (4-iodo-Phe), carboxylic acid (Asp), and N-donor (His).

An A4S mutation introduces a hydroxyl group and preserved the general framework structure, crystallizing in a nearly identical unit cell (Figure 3b). The Ser side-chain points directly into the large pore enabling the hydroxyl group to H-bond with a nearby O atom on BPE1. This result is noteworthy as it shows that introduction of a potent H-bond donor and acceptor sidechain does not interrupt the interactions that stabilize the lattice. However, a mutation to a thioether-containing side-chain in the A4M mutant crystallized in a different, non-porous structure. Although mutagenesis simulations suggested that methionine's sidechain could exist in the space of the pore, the SC-XRD of **UIC-1-A4M** revealed that attractive π-S interactions between BPH/BPE with the thioether induced an alternative tightly packed crystal (Figure S26).[53]

We hypothesized that methionine at positions 5 and 7, which are further away from bipyridine moieties, could maintain the framework. Indeed, both **UIC-1-B5M** and **UIC-1-B7M** crystallized in a similar unit cell to **UIC-1** and had the same framework topology. The main difference between **UIC-1-B5M** and **UIC-1-B7M** is that the Met side chain on B7M points more deeply into the minor crevice and excludes the MeCN that had occupied that pore in **UIC-1**, whereas in **UIC-1-B5M**, the sidechain is angled more into the main channel (Figure 3b).

Next, we explored whether more reactive acidic and basic functionalities could display in the pore, which has not previously been demonstrated in peptide-metal frameworks (Figure 3b). The B5D mutation (**UIC-1-B5D**) introduces a carboxylic acid and successfully forms the correct framework. Asp5 points into the major pore and forms hydrogen bonds with two water molecules within the pore. Conversely, the B5H mutation (**UIC-1-B5H**) appends a basic N-atom donor pointing into the main channel. The His residue is

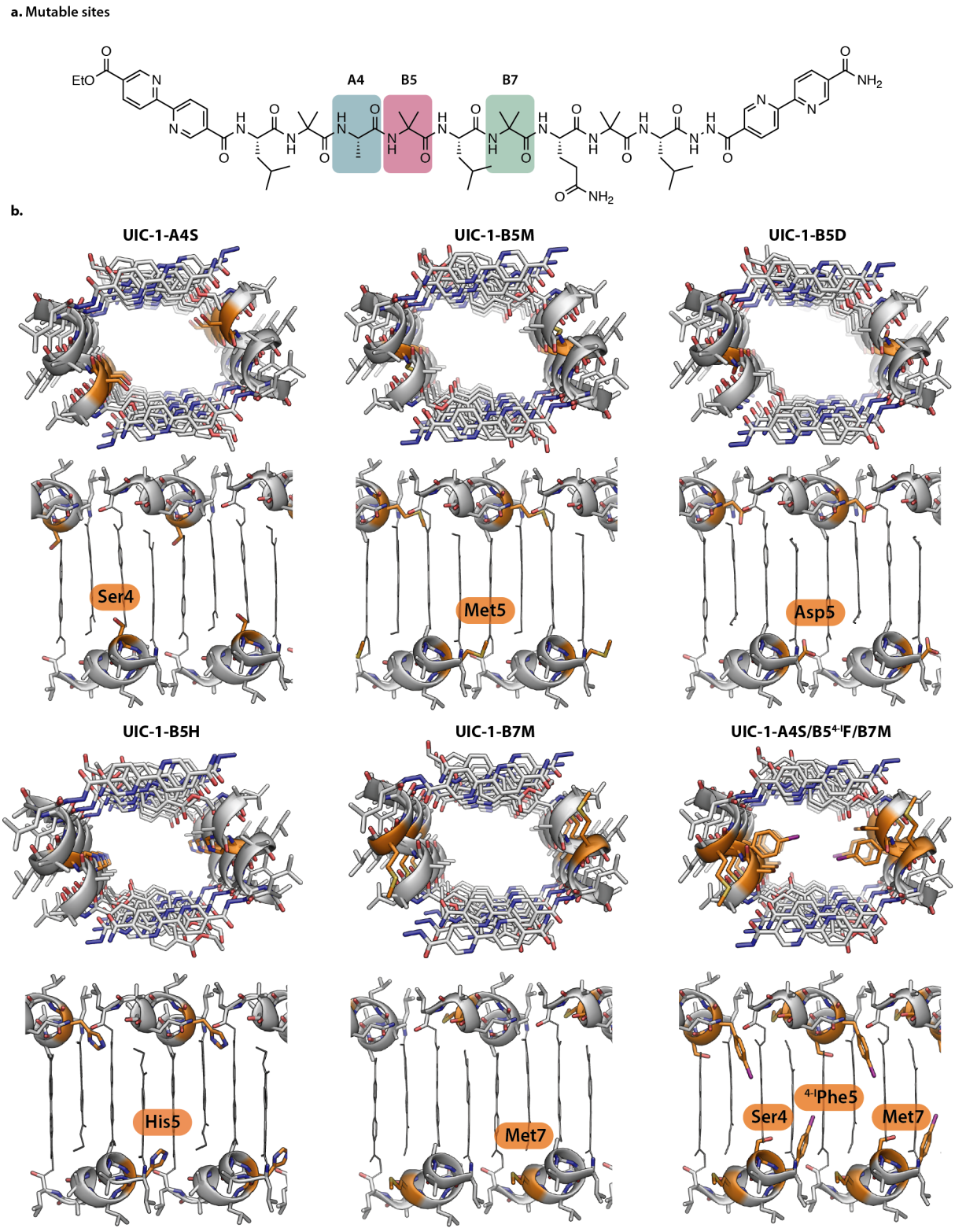

Figure 3. X-ray crystal structures of the **UIC-1** mutants showing pore views down the *b* and *a* axes. Mutated sites are highlighted in orange.

neutral and hydrogen bonds with a water molecule and the amide carbonyl of BPE.

Lastly, we tested whether **UIC-1** could simultaneously tolerate multiple, functionally diverse mutations. A triple mutant (**UIC-1-A4S/B5$^{4\text{-I}}$F/B7M**) consisting of hydrogen-bonding, aromatic, and thioether residues (mutations A4S, B5$^{4\text{-iodo}}$F, and B7M), remarkably crystallized in the same topology as observed in **UIC-1**. Both Ser4 and $^{4\text{-I}}$Phe5 sidechains point into the main channel, while the sidechain of Met7 is directed into the minor pore

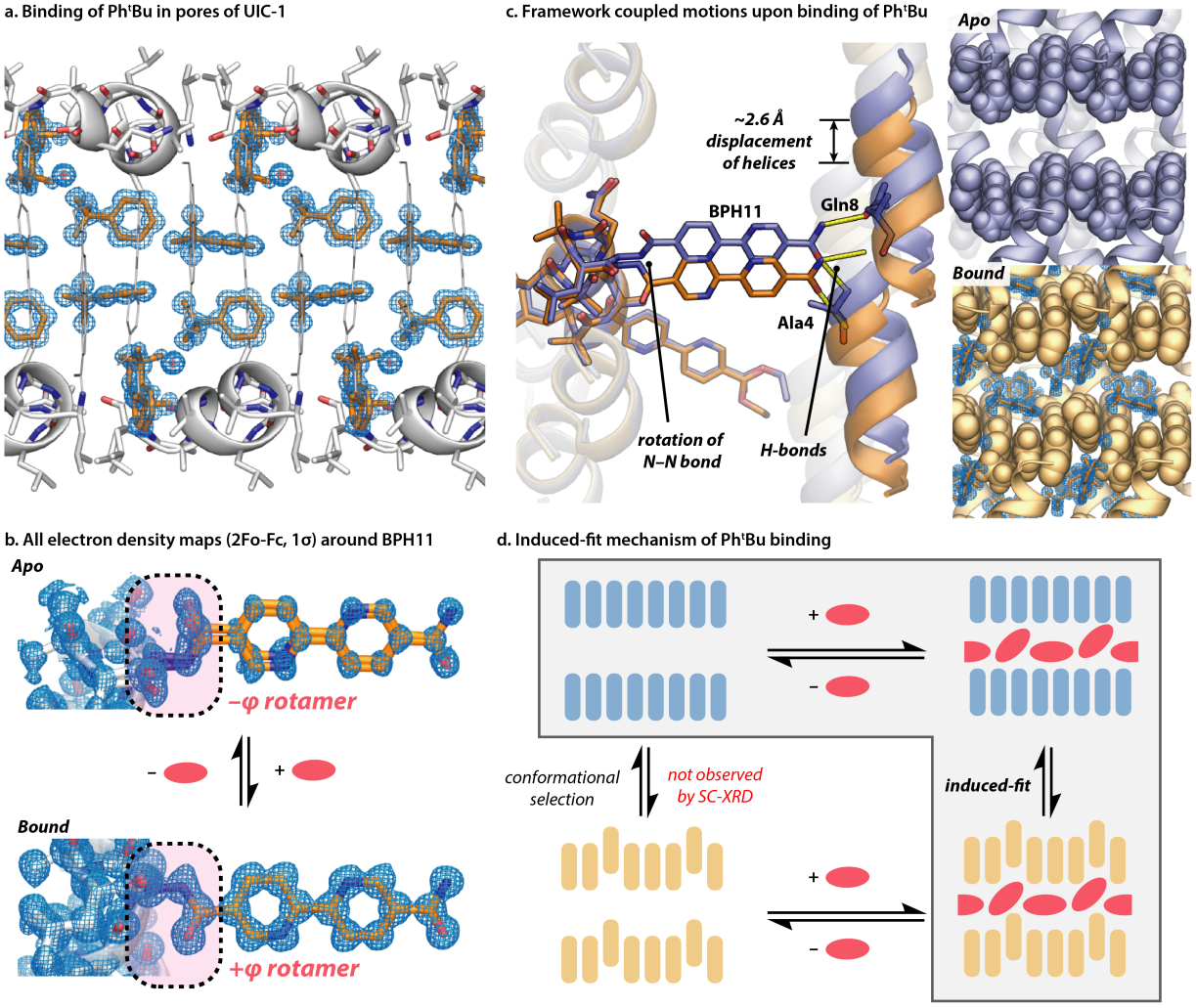

Figure 4. (a) X-ray crystal structure of **UIC-1⊂PhᵗBu** showing the electron density map of PhᵗBu guest molecules within the main channel. (b) Electron density maps highlighting the drastic rotation of BPH11's dihedral angle upon guest-binding in **UIC-1**. (c) Overlay of X-ray crystal structures of apo **UIC-1** (orange) and **UIC-1⊂PhᵗBu** (blue). Upon guest-binding, BPH11's N-N bond rotates while dragging an opposing helix upward to maintain a H-bond with Gln8. (d) Graphical illustration of **UIC-1**'s ability to perform an induced-fit mechanism upon PhᵗBu binding. The framework along the channel becomes corrugated as a direct result of helical translations during guest-uptake.

(Figure 3b). Thus, **UIC-1-A4S/B5$^{4\text{-iodo}}$F/B7M** reveals the extensive modularity achievable via peptidic frameworks, where the pore can accommodate an unprecedented level of mutations of varying functionalities.

We postulated that **UIC-1** would be a good candidate for host-guest chemistry due to the size of its pores. Host-guest chemistry is a key milestone en route to materials that could act as artificial enzymes or highly selective absorbents. Additionally, stability in water is highly desirable, as it is an important trait for applications of porous materials.[54] As previously mentioned, several H_2O and MeCN molecules are present in the large pore and minor crevices of **UIC-1** upon synthesis. This suggested that this material could tolerate aqueous and organic environments, and indeed the crystals showed no obvious physical changes when soaked in H_2O or certain organic solvents (acetonitrile, ethyl acetate, benzene, tetrahydrofuran, and dichloromethane), even after several weeks. The synergy of hydrophobic and hydrophilic interactions revealed by the crystal structure of **UIC-1** provides a rationale for the stability of this framework in a variety of solvents. Only highly polar organic solvents such as MeOH, dimethyl sulfoxide, and *N,N*-dimethylformamide are able to dissolve the framework.

Given the large pore dimensions, we challenged **UIC-1** to absorb decently sized, aromatic guests. First, **UIC-1** was soaked with a neat tert-butylbenzene (PhᵗBu) solution for several days. SC-XRD shows that UIC-1 maintains its crystallinity and contains three molecules of PhᵗBu per **UIC-1** molecule (Figure 4a). Two of these guests are arranged in a highly ordered fashion throughout the main channel without any disruption of π-π stacking between BPE and BPH or the peptidyl backbone. The third PhᵗBu molecule nestles itself in the minor pore, which exists in two orientations with 41% and 59% occupancies, either with the aromatic ring or t-butyl group inserted into the pocket, respectively. Addition of PhᵗBu also expels all but one water molecule, which is H-bonded to BPH.

Notably, the pores of **UIC-1** greatly reshape upon binding of PhᵗBu. In **UIC-1⊂PhᵗBu**, the N–N bond in BPH rotates by nearly 140°, which in turn causes a strong corrugation bipyridyl π-stacking

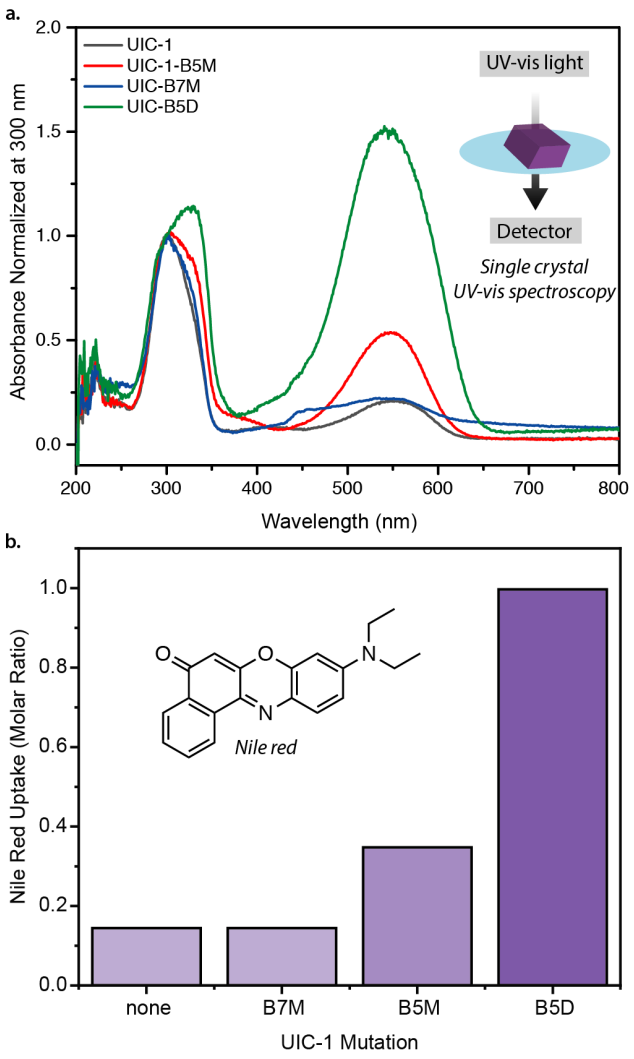

Figure 5. (a) Single-crystal UV-vis spectroscopy of variants after soaking with Nile red. (b) Quantification of Nile red uptake by UV-vis spectroscopy (see Supporting Information for details).

in the main channel. The C–N–N–C torsion is −54° (−φ state) and +85.6° (+φ state) for the apo and bound states, respectively. Since BPH hydrogen-bonds to two other chains (*vide supra*), this extreme rotation results in a significant displacement of the helices (~2.6 Å) (Figure 4b and 4c). Thus, the binding of Ph^{t}Bu but **UIC-1** is consistent with an induced-fit binding mechanism (guest binding triggers conformational changes in host) (Figure 4d) commonly used by proteins to enhance selectivity and is also seen in some metal-organic frameworks.[55,56] An alternative "conformational selection" mechanism, which has been previously observed in peptide-metal frameworks,[20,22] is less probable in this case as the crystal structure of **UIC-1** shows no electron-density for alternative conformations resembling those in **UIC-1⊂Ph^{t}Bu** (Figure 4b).[57]

We then tested the adsorption of iodobenzene, PhI, a slightly smaller guest than Ph^{t}Bu. Surprisingly, SC-XRD identifies only one PhI molecule with 67% total occupancy embedded within the minor pore of **UIC-1** (Supporting Information). However, no electron density from additional PhI was found in the large channel despite the fact that this crystal was soaked in neat PhI indicating that PhI is highly disordered within the larger pore. Only 30% of the BPH exists in the +φ conformation, suggesting that **UIC-1** and PhI are not well-matched hosts and guests, and induced-fit happens to a far lesser extent than with Ph^{t}Bu. The level of helical displacements is also less in **UIC-1⊂PhI**, which only moved the opposing helix by 1.1 Å (*vide supra*). This is noteworthy given the slight size differences between PhI and Ph^{t}Bu, and showcases how **UIC-1** can distinguish between these two similar molecules using induced-fit.

Given that **UIC-1** could accommodate up to three benzene-type molecules per peptide, we tested whether a larger molecule could fit, like Nile red, which has four-fused sp^2 rings decorated with heteroatoms. Crystals of **UIC-1**, **UIC-1-B5M**, **UIC-1-B7M**, and **UIC-1-B5D** were soaked in a solution of Nile red in MeCN (~1 mg/mL), and they took on different shades and intensities of purple or pink depending on the mutant (Figure 5).[58] UV-vis absorption spectra of individual crystals showed that **UIC-B5D** has a much higher affinity for the dye than rest of the variants, which is also consistent with the much darker appearance of the crystals (Figure 5 and S25). Though SC-XRD did not show clear density for Nile red in the pore (possibly due to high disorder), we propose that the aspartic acid residue of B5D mutant better interacts with the dye via hydrogen-bonds to O or N atoms of Nile red. This result is a proof-of-principle that the pores of **UIC-1** can be readily mutated to evolve desired properties.

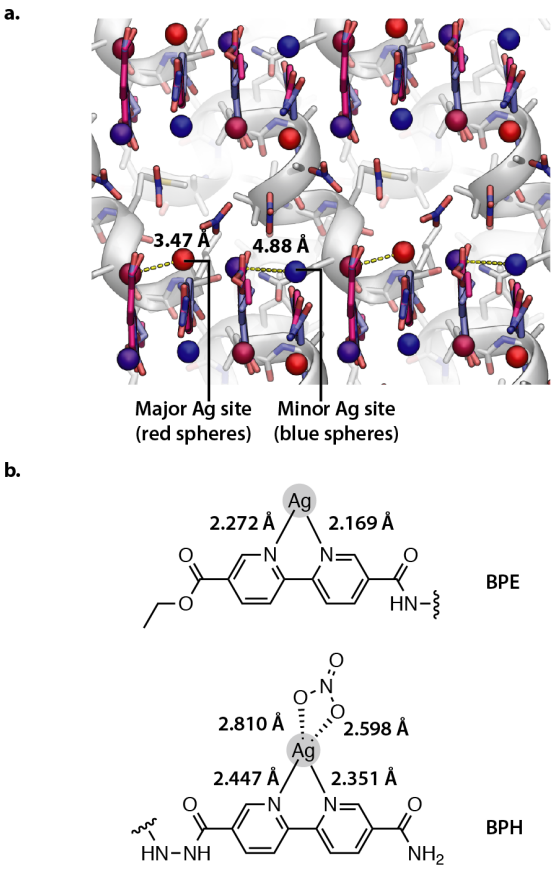

Figure 6. (a) X-ray crystal structure showing the arrangement of Ag^+ ions within **UIC-1-B7M⊂2AgNO$_3$**. Ag sites are colored by occupancy (red-blue gradient). The major (69 and 60% occupancy) and minor (31 and 40% occupancy) Ag sites are indicated by red and blue spheres, respectively. Ag–Ag distances are labeled. (b) Bond distances of Ag–ligand interactions.

Lastly, we tested whether the bipyridine motifs, which are well-established strong metal-binding ligands, could coordinate transition metal ions to the framework. Demonstrating that metal ions can bind to the protein-like framework creates opportunities to mimic or model metalloprotein active sites. Initial attempts of soaking crystals with 0.1 M $CoCl_2$ or $CuCl_2$ in water showed no binding of Co(II) (by SC-XRD), whereas prolonged exposure to excess Cu(II) degraded the crystals. However, **UIC-1-B7M** soaked with 0.1 M $AgNO_3$ showed high incorporation of Ag(I) ions (two Ag per peptide), as determined by SC-XRD. Ag(I) ions are chelated by BPH and BPE residues and are disordered over a major and minor site (major site occupancies of 69% and 60%; minor site occupancies of 31% and 40%) (Figure 6a). The major Ag sites form $[Ag_2]^{2+}$ clusters having an Ag–Ag distance of 3.446 Å, which is within the range of argentophilic interactions.[59] Ag–ligand distances and angles are consistent with previous examples (Figure 6b).[60,61] We hypothesize that favorable Ag(I) uptake could be due to the lower Coulombic repulsions of the +1 ion and the ability to form argentophilic interactions. The ability for the framework to host catalytically-active metal ions and even multi-metallic assemblies considerably expands the functional space of this material.[62]

CONCLUSIONS

We have reported a robust strategy to significantly advance the capabilities of peptide-frameworks. By enabling mutagenesis of multiple distinct positions in the channel, the number of pore environments grows exponentially. Notably, we show that π-stacking by polyaromatic residues is a reliable, metal-free interaction that will be useful for future designs of non-covalent frameworks.[40] The π-stacking, metal-free strategy is critical for tolerating useful functional groups containing carboxylic acids, N- and S-donors, which are rarely compatible with metal-coordination frameworks. Furthermore, the flexibility afforded by non-covalent assembly facilitates conformationally dynamic, protein-like engagement with guest molecules. Though non-covalent forces drive framework assembly, metal ions can also be added post-synthetically to create metalloprotein-like active sites.

Most crucially, while previous peptide-frameworks had few opportunities for mutagenesis, the materials reported herein are readily evolvable, as illustrated by the identification of a variant that can strongly bind a complex organic molecule. The speed and ease of peptide variation, combined with the plurality of mutable residues in **UIC-1** provides a reliable mechanism going forward to discover novel functions by rational or combinatorial design.

ASSOCIATED CONTENT

Supporting Information

Synthetic, spectroscopic, and crystallographic details are provided in the Supporting Information, and is available free of charge on the ACS Publications website.

AUTHOR INFORMATION

Corresponding Author

* andyn@uic.edu

Author Contributions

‡These authors contributed equally.

ACKNOWLEDGMENT

This research was supported by start-up funds from the University of Illinois at Chicago. A.P. was supported by the UIC Honors College Research Grant and the UIC Chancellor's Undergraduate Research Award (CURA). This research used resources of the Advanced Photon Source, a U.S. Department of Energy (DOE) Office of Science User Facility operated for the DOE Office of Science by Argonne National Laboratory under Contract No. DE-AC02-06CH11357. Use of the LS-CAT Sector 21 was supported by the Michigan Economic Development Corporation and the Michigan Technology Tri-Corridor (Grant 085P1000817). Data were collected at the Life Sciences Collaborative Access Team beamline 21-ID-D and 21-ID-G at the Advanced Photon Source, Argonne National Laboratory. We thank Prof. Xiaojing Yang, Prof. Neal Mankad, Pinar Alayoglu, and Hsien-Cheng Yu for assistance with the collection of single crystal X-ray diffraction data and Prof. Stephanie Cologna for assistance with mass spectrometry data.

REFERENCES

(1) Stank, A.; Kokh, D. B.; Fuller, J. C.; Wade, R. C. Protein Binding Pocket Dynamics. *Acc. Chem. Res.* **2016**, *49* (5), 809–815. https://doi.org/10.1021/acs.accounts.5b00516.

(2) Otvos, L.; Wade, J. D. Current Challenges in Peptide-Based Drug Discovery. *Frontiers in Chemistry* **2014**, *2*, 62. https://doi.org/10.3389/fchem.2014.00062.

(3) Eck, R. V.; Dayhoff, M. O. Evolution of the Structure of Ferredoxin Based on Living Relics of Primitive Amino Acid Sequences. *Science* **1966**, *152* (3720), 363–366. https://doi.org/10.1126/science.152.3720.363.

(4) Romero Romero, M. L.; Rabin, A.; Tawfik, D. S. Functional Proteins from Short Peptides: Dayhoff's Hypothesis Turns 50. *Angewandte Chemie International Edition* **2016**, *55* (52), 15966–15971. https://doi.org/10.1002/anie.201609977.

(5) D'Alessio, G. The Evolutionary Transition from Monomeric to Oligomeric Proteins: Tools, the Environment, Hypotheses. *Progress in Biophysics and Molecular Biology* **1999**, *72* (3), 271–298. https://doi.org/10.1016/S0079-6107(99)00009-7.

(6) Alva, V.; Lupas, A. N. From Ancestral Peptides to Designed Proteins. *Curr Opin Struct Biol* **2018**, *48*, 103–109. https://doi.org/10.1016/j.sbi.2017.11.006.

(7) Yadid, I.; Kirshenbaum, N.; Sharon, M.; Dym, O.; Tawfik, D. S. Metamorphic Proteins Mediate Evolutionary Transitions of Structure. *PNAS* **2010**, *107* (16), 7287–7292. https://doi.org/10.1073/pnas.0912616107.

(8) Rufo, C. M.; Moroz, Y. S.; Moroz, O. V.; Stöhr, J.; Smith, T. A.; Hu, X.; DeGrado, W. F.; Korendovych, I. V. Short Peptides Self-Assemble to Produce Catalytic Amyloids. *Nature Chem* **2014**, *6* (4), 303–309. https://doi.org/10.1038/nchem.1894.

(9) Zastrow, M. L.; Peacock, A. F. A.; Stuckey, J. A.; Pecoraro, V. L. Hydrolytic Catalysis and Structural Stabilization in a Designed Metalloprotein. *Nature Chemistry* **2012**, *4* (2), 118–123. https://doi.org/10.1038/nchem.1201.

(10) Morimoto, M.; Bierschenk, S. M.; Xia, K. T.; Bergman, R. G.; Raymond, K. N.; Toste, F. D. Advances in Supramolecular Host-Mediated Reactivity. *Nat Catal* **2020**, *3* (12), 969–984. https://doi.org/10.1038/s41929-020-00528-3.

(11) Zhou, H.-C.; Long, J. R.; Yaghi, O. M. Introduction to Metal–Organic Frameworks. *Chem. Rev.* **2012**, *112* (2), 673–674. https://doi.org/10.1021/cr300014x.

(12) Zhu, J.; Avakyan, N.; Kakkis, A.; Hoffnagle, A. M.; Han, K.; Li, Y.; Zhang, Z.; Choi, T. S.; Na, Y.; Yu, C.-J.; Tezcan, F. A. Protein Assembly by Design. *Chem. Rev.* **2021**, *121* (22), 13701–13796. https://doi.org/10.1021/acs.chemrev.1c00308.

(13) Collins, J. M.; Porter, K. A.; Singh, S. K.; Vanier, G. S. High-Efficiency Solid Phase Peptide Synthesis (HE-SPPS). *Org. Lett.* **2014**, *16* (3), 940–943. https://doi.org/10.1021/ol4036825.

(14) Mijalis, A. J.; Iii, D. A. T.; Simon, M. D.; Adamo, A.; Beaumont, R.; Jensen, K. F.; Pentelute, B. L. A Fully Automated Flow-Based Approach for Accelerated Peptide Synthesis. *Nature Chemical Biology* **2017**, *13* (5), 464–466. https://doi.org/10.1038/nchembio.2318.

(15) Horne, W. S.; Grossmann, T. N. Proteomimetics as Protein-Inspired Scaffolds with Defined Tertiary Folding Patterns. *Nat. Chem.* **2020**, *12* (4), 331–337. https://doi.org/10.1038/s41557-020-0420-9.

(16) Schnitzer, T.; Paenurk, E.; Trapp, N.; Gershoni-Poranne, R.; Wennemers, H. Peptide–Metal Frameworks with Metal Strings Guided by Dispersion Interactions. *J. Am. Chem. Soc.* **2021**, *143* (2), 644–648. https://doi.org/10.1021/jacs.0c11793.

(17) Saito, A.; Sawada, T.; Fujita, M. X-Ray Crystallographic Observation of Chiral Transformations within a Metal–Peptide Pore. *Angewandte Chemie International Edition* **2020**, *59* (46), 20367–20370. https://doi.org/10.1002/anie.202007731.

(18) Sawada, T.; Matsumoto, A.; Fujita, M. Coordination-Driven Folding and Assembly of a Short Peptide into a Protein-like Two-Nanometer-Sized Channel. *Angewandte Chemie* **2014**, *126* (28), 7356–7360. https://doi.org/10.1002/ange.201403506.

(19) Navarro-Sánchez, J.; Argente-García, A. I.; Moliner-Martínez, Y.; Roca-Sanjuán, D.; Antypov, D.; Campíns-Falcó, P.; Rosseinsky, M. J.; Martí-Gastaldo, C. Peptide Metal–Organic Frameworks for Enantioselective Separation of Chiral Drugs. *J. Am. Chem. Soc.* **2017**, *139* (12), 4294–4297. https://doi.org/10.1021/jacs.7b00280.

(20) Rabone, J.; Yue, Y.-F.; Chong, S. Y.; Stylianou, K. C.; Bacsa, J.; Bradshaw, D.; Darling, G. R.; Berry, N. G.; Khimyak, Y. Z.; Ganin, A. Y.; Wiper, P.; Claridge, J. B.; Rosseinsky, M. J. An Adaptable Peptide-Based Porous Material. *Science* **2010**. https://doi.org/10.1126/science.1190672.

(21) Martí-Gastaldo, C.; Antypov, D.; Warren, J. E.; Briggs, M. E.; Chater, P. A.; Wiper, P. V.; Miller, G. J.; Khimyak, Y. Z.; Darling, G. R.; Berry, N. G.; Rosseinsky, M. J. Side-Chain Control of Porosity Closure in Single- and Multiple-Peptide-Based Porous Materials by Cooperative Folding. *Nature Chemistry* **2014**, *6* (4), 343–351. https://doi.org/10.1038/nchem.1871.

(22) Katsoulidis, A. P.; Antypov, D.; Whitehead, G. F. S.; Carrington, E. J.; Adams, D. J.; Berry, N. G.; Darling, G. R.; Dyer, M. S.; Rosseinsky, M. J. Chemical Control of Structure and Guest Uptake by a Conformationally Mobile Porous Material. *Nature* **2019**, *565* (7738), 213–217. https://doi.org/10.1038/s41586-018-0820-9.

(23) Yan, Y.; Carrington, E. J.; Pétuya, R.; Whitehead, G. F. S.; Verma, A.; Hylton, R. K.; Tang, C. C.; Berry, N. G.; Darling, G. R.; Dyer, M. S.; Antypov, D.; Katsoulidis, A. P.; Rosseinsky, M. J. Amino Acid Residues Determine the Response of Flexible Metal–Organic Frameworks to Guests. *J. Am. Chem. Soc.* **2020**, *142* (35), 14903–14913. https://doi.org/10.1021/jacs.0c03853.

(24) Misra, R.; Saseendran, A.; Dey, S.; Gopi, H. N. Metal-Helix Frameworks from Short Hybrid Peptide Foldamers. *Angewandte Chemie International Edition* **2019**, *58* (8), 2251–2255. https://doi.org/10.1002/anie.201810849.

(25) Mantion, A.; Massüger, L.; Rabu, P.; Palivan, C.; McCusker, L. B.; Taubert, A. Metal–Peptide Frameworks (MPFs): "Bioinspired" Metal Organic Frameworks. *J. Am. Chem. Soc.* **2008**, *130* (8), 2517–2526. https://doi.org/10.1021/ja0762588.

(26) Miyake, R.; Tashiro, S.; Shiro, M.; Tanaka, K.; Shionoya, M. Ni(II)-Mediated Self-Assembly of Artificial β-Dipeptides Forming a Macrocyclic Tetranuclear Complex with Interior Spaces for In-Line Molecular Arrangement. *J. Am. Chem. Soc.* **2008**, *130* (17), 5646–5647. https://doi.org/10.1021/ja8009555.

(27) Sawada, T.; Saito, A.; Tamiya, K.; Shimokawa, K.; Hisada, Y.; Fujita, M. Metal–Peptide Rings Form Highly Entangled Topologically Inequivalent Frameworks with the Same Ring- and Crossing-Numbers. *Nat Commun* **2019**, *10* (1), 921. https://doi.org/10.1038/s41467-019-08879-7.

(28) Chen, Y.; Yang, Y.; Orr, A. A.; Makam, P.; Redko, B.; Haimov, E.; Wang, Y.; Shimon, L. J. W.; Rencus-Lazar, S.; Ju, M.; Tamamis, P.; Dong, H.; Gazit, E. Self-Assembled Peptide Nano-Superstructure towards Enzyme Mimicking Hydrolysis. *Angew. Chem. Int. Ed.* **2021**, *60* (31), 17164–17170. https://doi.org/10.1002/anie.202105830.

(29) Chen, Y.; Guerin, S.; Yuan, H.; O'Donnell, J.; Xue, B.; Cazade, P.-A.; Haq, E. U.; Shimon, L. J. W.; Rencus-Lazar, S.; Tofail, S. A. M.; Cao, Y.; Thompson, D.; Yang, R.; Gazit, E. Guest Molecule-Mediated Energy Harvesting in a Conformationally Sensitive Peptide–Metal Organic Framework. *J. Am. Chem. Soc.* **2022**. https://doi.org/10.1021/jacs.1c11750.

(30) Imaz, I.; Rubio-Martínez, M.; An, J.; Solé-Font, I.; Rosi, N. L.; Maspoch, D. Metal–Biomolecule Frameworks (MBioFs). *Chem. Commun.* **2011**, *47* (26), 7287–7302. https://doi.org/10.1039/C1CC11202C.

(31) Dong, J.; Liu, Y.; Cui, Y. Artificial Metal–Peptide Assemblies: Bioinspired Assembly of Peptides and Metals through Space and across Length Scales. *J. Am. Chem. Soc.* **2021**, *143* (42), 17316–17336. https://doi.org/10.1021/jacs.1c08487.

(32) Peptide Metal–Organic Frameworks for Enantioselective Separation of Chiral Drugs | Journal of the American Chemical Society https://pubs.acs.org/doi/10.1021/jacs.7b00280 (accessed 2021 -12 -15).

(33) Bonnefoy, J.; Legrand, A.; Quadrelli, E. A.; Canivet, J.; Farrusseng, D. Enantiopure Peptide-Functionalized Metal–Organic Frameworks. *J. Am. Chem. Soc.* **2015**, *137* (29), 9409–9416. https://doi.org/10.1021/jacs.5b05327.

(34) Magnotti, E. L.; Hughes, S. A.; Dillard, R. S.; Wang, S.; Hough, L.; Karumbamkandathil, A.; Lian, T.; Wall, J. S.; Zuo, X.; Wright, E. R.; Conticello, V. P. Self-Assembly of an α-Helical Peptide into a Crystalline Two-Dimensional Nanoporous Framework. *J. Am. Chem. Soc.* **2016**, *138* (50), 16274–16282. https://doi.org/10.1021/jacs.6b06592.

(35) Tavenor, N. A.; Murnin, M. J.; Horne, W. S. Supramolecular Metal-Coordination Polymers, Nets, and Frameworks from Synthetic Coiled-Coil Peptides. *J. Am. Chem. Soc.* **2017**, *139* (6), 2212–2215. https://doi.org/10.1021/jacs.7b00651.

(36) Nepal, M.; Sheedlo, M. J.; Das, C.; Chmielewski, J. Accessing Three-Dimensional Crystals with Incorporated Guests through Metal-Directed Coiled-Coil Peptide Assembly. *J. Am. Chem. Soc.* **2016**, *138* (34), 11051–11057. https://doi.org/10.1021/jacs.6b06708.

(37) Teng, P.; Niu, Z.; She, F.; Zhou, M.; Sang, P.; Gray, G. M.; Verma, G.; Wojtas, L.; van der Vaart, A.; Ma, S.; Cai, J. Hydrogen-Bonding-Driven 3D Supramolecular Assembly of Peptidomimetic Zipper. *J. Am. Chem. Soc.* **2018**, *140* (17), 5661–5665. https://doi.org/10.1021/jacs.7b11997.

(38) Chen, K. H.; Corro, K. A.; Le, S. P.; Nowick, J. S. X-Ray Crystallographic Structure of a Giant Double-Walled Peptide Nanotube Formed by a Macrocyclic β-Sheet Containing Aβ16–22. *J. Am. Chem. Soc.* **2017**, *139* (24), 8102–8105. https://doi.org/10.1021/jacs.7b03890.

(39) Yoo, S.; Kreutzer, A. G.; Truex, N. L.; Nowick, J. S. Square Channels Formed by a Peptide Derived from Transthyretin. *Chem. Sci.* **2016**, *7* (12), 6946–6951. https://doi.org/10.1039/C6SC01927G.

(40) Deng, J.-H.; Luo, J.; Mao, Y.-L.; Lai, S.; Gong, Y.-N.; Zhong, D.-C.; Lu, T.-B. π-π Stacking Interactions: Non-Negligible Forces for Stabilizing Porous Supramolecular Frameworks. *Science Advances* **2020**, *6* (2), eaax9976. https://doi.org/10.1126/sciadv.aax9976.

(41) Haimov, B.; Srebnik, S. A Closer Look into the α-Helix Basin. *Sci Rep* **2016**, *6* (1), 38341. https://doi.org/10.1038/srep38341.

(42) Garner, J.; Harding, M. M. Design and Synthesis of α-Helical Peptides and Mimetics. *Org. Biomol. Chem.* **2007**, *5* (22), 3577. https://doi.org/10.1039/b710425a.

(43) Karle, I. L.; Balaram, P. Structural Characteristics of .Alpha.-Helical Peptide Molecules Containing Aib Residues. *Biochemistry* **1990**, *29* (29), 6747–6756. https://doi.org/10.1021/bi00481a001.

(44) Mondal, S.; Varenik, M.; Bloch, D. N.; Atsmon-Raz, Y.; Jacoby, G.; Adler-Abramovich, L.; Shimon, L. J. W.; Beck, R.; Miller, Y.; Regev, O.; Gazit, E. A Minimal Length Rigid Helical Peptide Motif Allows Rational Design of Modular Surfactants. *Nature Communications* **2017**, *8*, 14018. https://doi.org/10.1038/ncomms14018.

(45) Itagaki, T.; Uji, H.; Imai, T.; Kimura, S. Sterical Recognition at Helix–Helix Interface of Leu-Aib-Based Polypeptides with and without a GxxxG-Motif. *Langmuir* **2019**, *35* (22), 7249–7254. https://doi.org/10.1021/acs.langmuir.9b00620.

(46) Tovar, J. D. Supramolecular Construction of Optoelectronic Biomaterials. *Acc. Chem. Res.* **2013**, *46* (7), 1527–1537. https://doi.org/10.1021/ar3002969.

(47) Lewandowska, U.; Zajaczkowski, W.; Corra, S.; Tanabe, J.; Borrmann, R.; Benetti, E. M.; Stappert, S.; Watanabe, K.; Ochs, N. A. K.; Schaeublin, R.; Li, C.; Yashima, E.; Pisula, W.; Müllen, K.; Wennemers, H. A Triaxial Supramolecular Weave. *Nature Chem* **2017**, *9* (11), 1068–1072. https://doi.org/10.1038/nchem.2823.

(48) Ashkenasy, N.; Horne, W. S.; Ghadiri, M. R. Design of Self-Assembling Peptide Nanotubes with Delocalized Electronic States. *Small* **2006**, *2* (1), 99–102. https://doi.org/10.1002/smll.200500252.

(49) Kumar, R. J.; MacDonald, J. M.; Singh, Th. B.; Waddington, L. J.; Holmes, A. B. Hierarchical Self-Assembly of Semiconductor Functionalized Peptide α-Helices and Optoelectronic Properties. *J. Am. Chem. Soc.* **2011**, *133* (22), 8564–8573. https://doi.org/10.1021/ja110858k.

(50) Janiak, C. A Critical Account on π–π Stacking in Metal Complexes with Aromatic Nitrogen-Containing Ligands. *J. Chem. Soc., Dalton Trans.* **2000**, No. 21, 3885–3896. https://doi.org/10.1039/B003010O.

(51) Dey, S.; Misra, R.; Saseendran, A.; Pahan, S.; Gopi, H. N. Metal-Coordinated Supramolecular Polymers from the Minimalistic Hybrid Peptide Foldamers. *Angewandte Chemie International Edition* **2021**, *60* (18), 9863–9868. https://doi.org/10.1002/anie.202015838.

(52) Martí-Gastaldo, C.; Warren, J. E.; Briggs, M. E.; Armstrong, J. A.; Thomas, K. M.; Rosseinsky, M. J. Sponge-Like Behaviour in Isoreticular Cu(Gly-His-X) Peptide-Based Porous Materials. *Chemistry – A European Journal* **2015**, *21* (45), 16027–16034. https://doi.org/10.1002/chem.201502098.

(53) Forbes, C. R.; Sinha, S. K.; Ganguly, H. K.; Bai, S.; Yap, G. P. A.; Patel, S.; Zondlo, N. J. Insights into Thiol–Aromatic Interactions: A Stereoelectronic Basis for S–H/π Interactions. *J. Am. Chem. Soc.* **2017**, *139* (5), 1842–1855. https://doi.org/10.1021/jacs.6b08415.

(54) Water Stability and Adsorption in Metal–Organic Frameworks | Chemical Reviews https://pubs.acs.org/doi/abs/10.1021/cr5002589 (accessed 2021 -12 -16).

(55) Koshland, D. E. Application of a Theory of Enzyme Specificity to Protein Synthesis*. *Proc Natl Acad Sci U S A* **1958**, *44* (2), 98–104.

(56) Schneemann, A.; Bon, V.; Schwedler, I.; Senkovska, I.; Kaskel, S.; Fischer, R. A. Flexible Metal–Organic Frameworks. *Chem. Soc. Rev.* **2014**, *43* (16), 6062–6096. https://doi.org/10.1039/C4CS00101J.

(57) Paul, F.; Weikl, T. R. How to Distinguish Conformational Selection and Induced Fit Based on Chemical Relaxation Rates. *PLoS Comput Biol* **2016**, *12* (9), e1005067. https://doi.org/10.1371/journal.pcbi.1005067.

(58) Greenspan, P.; Fowler, S. D. Spectrofluorometric Studies of the Lipid Probe, Nile Red. *Journal of Lipid Research* **1985**, *26* (7), 781–789. https://doi.org/10.1016/S0022-2275(20)34307-8.

(59) Schmidbaur, H.; Schier, A. Argentophilic Interactions. *Angewandte Chemie International Edition* **2015**, *54* (3), 746–784. https://doi.org/10.1002/anie.201405936.

(60) Lindley, P. F.; Woodward, P. An X-Ray Investigation of Silver Nitrate: A Unique Metal Nitrate Structure. *J. Chem. Soc. A* **1966**, No. 0, 123–126. https://doi.org/10.1039/J19660000123.

(61) Bellusci, A.; Crispini, A.; Pucci, D.; Szerb, E. I.; Ghedini, M. Structural Variations in Bipyridine Silver(I) Complexes: Role of the Substituents and Counterions. *Crystal Growth & Design* **2008**, *8* (8), 3114–3122. https://doi.org/10.1021/cg8003323.

(62) Dehghany, M.; Schomaker, J. M. Silver-Catalyzed Enantioselective Functionalizations of Alkenes and Alkynes: A Short Review. *Current Opinion in Green and Sustainable Chemistry* **2021**, *30*, 100483. https://doi.org/10.1016/j.cogsc.2021.100483.

TOC Graphic:

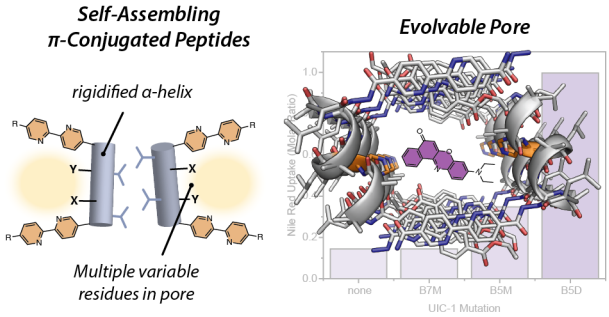
Self-Assembling
π-Conjugated Peptides
rigidified α-helix
Y
X
X
Y
Multiple variable
residues in pore
Evolvable Pore
1.0
0.0
none
B7M
B5M
B5D
UIC-1 Mutation